FUDMA Journal of Sciences (FJS)
ISSN online: 2616-1370
ISSN print: 2645 - 2944
Vol. 10 No. 15, August, 2026, pp 45 – 50
DOI: https://doi.org/10.33003/fjs-2026-1015-5848

Numerical Investigation of Seasonal Performance of an Indirect Solar Dryer Using CFD

[1]Anas Nomau Sabiyel and [2]Umar Muhammad Gana

[1]Department of Physics, Abdullahi Fodio University of Science and Technology, Aliero.
[2]Department of Physics, Bayero University, Kano.

*Corresponding authors' email: anas.nomausabiel@ksusta.edu.ng Phone: +2347089803939

ABSTRACT
This study presents a numerical investigation of the seasonal performance of an indirect solar dryer using computational fluid dynamics (CFD) in COMSOL Multiphysics 5.6. The simulated dryer was evaluated for the dry, harmattan and rainy seasons in Kano, Northwestern Nigeria using outlet air velocity and temperature distribution as the principal performance indicators. At 35 min of simulation time, the predicted maximum outlet velocities were 27.9 m/s, 23.5 m/s and 22.8 m/s for the dry, harmattan and rainy seasons respectively. The corresponding seasonal ambient temperatures used as simulation inputs were 36.0 °C, 31.75 °C and 32.0 °C. The simulations produced maximum temperature values of 416.71 K, 399.19 K and 388.15 K for the dry, harmattan and rainy seasons respectively. These peak values are the maximum velocity outlet and temperature distribution predicted by the CFD model and the results indicate that seasonal environmental conditions substantially influence the predicted airflow and thermal fields of the dryer with the dry season producing the highest outlet velocity and temperature values. The study demonstrates the usefulness of CFD for assessing seasonal airflow and thermal behaviour of an indirect solar dryer before physical construction.

Received: 01 July 2026
Accepted: 17 July 2026
Published: 31 Aug. 2026

Keywords: Indirect Solar Dryer, Numerical Simulation, Seasonal Performance, Flow Velocity and Temperature Distributions

INTRODUCTION

Drying is one of the oldest and most widely used methods for food preservation of agricultural products and during this old method people were using direct open sun drying with its numerous implications such as contamination by dust, pollution and damage by birds, animal, insects and some other bacteria (Patterson, 2018). Conventional drying techniques are mainly relying on fossil fuels or electricity leading to high operational costs and environmental concerns. An indirect solar dryer conventionally works by heating air in a separate solar collector then passing the warm air through a drying chamber containing the product so that the material is not exposed to direct sunlight. The system is considered as an alternative way for drying agricultural products due to its low cost, environmental friendliness and suitability for rural and agricultural applications (Demissie *et al.*, 2019). This type of solar drier has a better performance in terms of good dried product quality and reduced drying time.

Although CFD has been widely applied to the design and optimization of solar dryers, the studies cited in this work mainly focus on airflow and temperature distribution for particular dryer operating conditions only. The present study addresses the need for a seasonal numerical assessment of an indirect solar dryer by evaluating outlet airflow velocity and temperature distribution under dry, harmattan and rainy season conditions in Kano, Northwestern Nigeria. This seasonal comparison provides a basis for identifying how changes in environmental operating conditions affect the predicted airflow and thermal behaviour of the dryer before physical construction. Therefore, computational fluid dynamics (CFD) provides a useful numerical approach for investigating the airflow and heat transfer behaviour of solar dryers and for evaluating dryer performance before physical construction (Demissie *et al.*, 2019; Beyene, 2017).

However, the studies cited above mainly address particular dryer operating conditions rather than explicitly comparing the predicted outlet airflow velocity and temperature distribution under different seasonal conditions. This study therefore investigates the seasonal performance of an indirect solar dryer in Kano, Northwestern Nigeria by developing a three dimensional CFD model and evaluating outlet airflow velocity and temperature distribution for the dry, harmattan and rainy seasons. The specific objectives are to: (i) design an indirect solar dryer, (ii) develop and simulate a 3D CFD model, (iii) predict the outlet airflow velocity within the drying chamber and (iv) predict and validate the temperature distribution inside the solar dryer.

MATERIALS AND METHODS

In this work, the materials and method adopted are designed to numerically investigate the seasonal performance of an indirect solar dryer under different environmental conditions in Kano, Northwestern Nigeria.

Materials

The materials used for this study are software materials as the work is fully simulation. These materials are: geometry (three dimensional computer model of the solar dryer), a structured computational mesh, air as the working fluid, porous media as drying chamber area, boundary condition inputs, heat flux source terms applied on domain walls and turbulence model settings. All designed in the computational fluid dynamics (CFD) solver using COMSOL Multiphysics 5.6.

Method

The indirect solar dryer considered in this study consists of three main components: a solar collector, a drying chamber (trays) and an air flow system (inlet and outlet). The solar collector absorbs solar radiation and heats the air which then flows through the drying chamber where agricultural products will be placed. Flow air taking the moisture out through an outlet vent (chimney) to make the moisture removal continuous. The trays arrangement to allow uniform air flow was made in the drying cabinet having three trays as drying chambers. Dryer overall length: 2.00m, overall height: 1.30m, collector and absorber plate dimension: 0.8 × 0.5m, glass cover thickness: 0.005m, insulation total thickness: 0.05m, gap between absorber plate and glass cover: 0.5m, Gap between absorber plate and insulation: 0.05m, Number of trays: 3, Tray dimension: 0.7× 1.2 m, Distance between trays: 0.15m, tilt angle of the collector: 15° due south and chimney 0.15× 0.05m respectively. The designed indirect solar dryer in COMSOL environment was exposed to dry season parameters in first stage. The parameters were wind velocity outlet and temperature distribution of the dryer. The performance of the dryer during this season was evaluated using temperature distribution of the dryer enclosure and the outlet wind velocity as the performance metrics 1. The simulation was repeated in stages for three different seasons, dry season, harmattan season and rainy season. The performances of the dryer at these seasons were also determined.

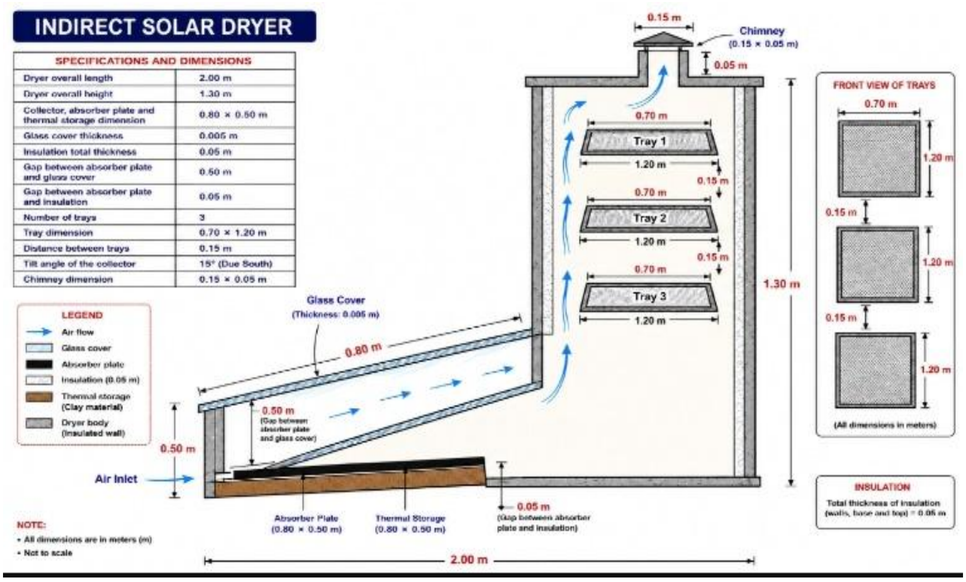

Figure 1: Detailed Designed and Dimensions of the Indirect Solar Dryer

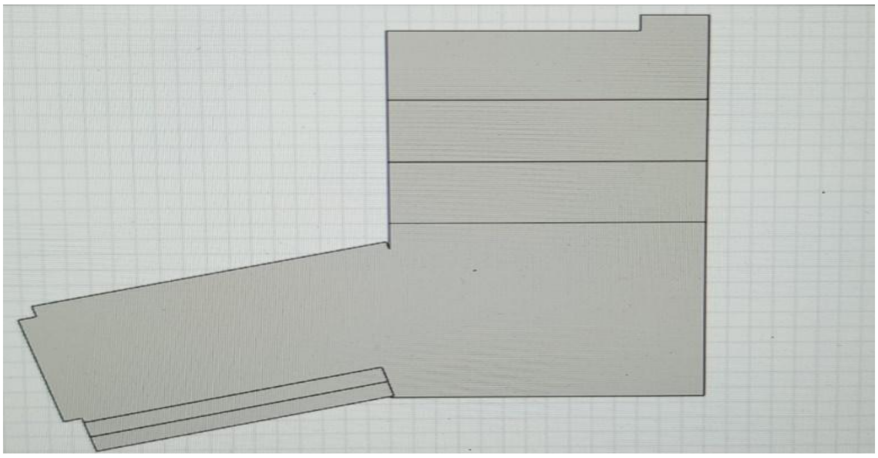

Figure 2: Designed of the Indirect Solar Dryer in the Simulation Model

Boundary Conditions and Seasonal Input Parameters

The CFD model used a velocity inlet boundary with seasonal air velocities of 7.86 m/s, 6.56 m/s, and 6.40 m/s and inlet temperatures of 36.0 °C (309.15 K), 31.75 °C (304.90 K) and 32.0 °C (305.15 K) for the dry, harmattan, and rainy seasons, respectively, while an outlet/open boundary was applied at the chimney. Seasonal absorber heat fluxes were 226.8 W/m², 205.0 W/m² and 185.7 W/m² corresponding to approximately 19.60 and 16.05 MJ/m²/day for the dry and rainy seasons respectively with heat flux directed normal to the absorber surface. External walls were insulated where heat losses were negligible, while fluid solid interfaces were coupled for conductive and convective heat transfer. Air properties in COMSOL Multiphysics 5.6 were temperature dependent with 1 atm (101,325 Pa) reference pressure and at approximately 300 K**,** density 1.18 kg/m³ dynamic viscosity 1.85×10^{-5} Pa·s**,** thermal conductivity 0.026 W/(m·K) and specific heat capacity 1005 J/(kg·K).

Solver Settings, Time Stepping and Convergence

The CFD model was solved as a transient time dependent problem in COMSOL Multiphysics 5.6 **for** 35 min (2100 s) using adaptive BDF time stepping a maximum time step of **10 s**, output interval of 60 s and final extraction at 2100 s. A relative tolerance of 1×10^{-3} and absolute tolerance of 1×10^{-6} were used with a fully coupled approach automatic damped Newton method, automatic Jacobian updates and PARDISO direct linear solver**.** Convergence was checked at every time step with the 10 s maximum allowing smaller adaptive steps when necessary and the 2100 s results accepted only after satisfying the prescribed convergence and error criteria.

CFD, Turbulence Model and Numerical Formulation

The airflow and heat transfer processes were simulated in COMSOL Multiphysics 5.6 using the CFD Module coupled with the Heat Transfer Module with the conservation of mass, momentum and energy solved simultaneously using the RANS k–ε turbulence model. Seasonal inlet velocities were 7.86 m/s, 6.56 m/s and 6.40 m/s with 5% turbulence intensity, a hydraulic diameter of 0.075 m and turbulence length scale of 0.0053 m based on inlet dimensions of 0.15 m × 0.05 m and 0.07L. The resulting turbulent kinetic energy values were 0.232, 0.161 and 0.154 m^2/s^2 while dissipation rates were 1.82, 1.05 and 0.99 m^2/s^3 for the dry, harmattan and rainy seasons respectively using $C\mu = 0.09$. The simulations were transient time dependent with air as the working fluid and coupled conductive convective heat transfer between fluid and solid domains while the three trays were treated as flow obstruction surfaces with no porous medium resistance, permeability or porosity parameters**.** The same CFD physics, turbulence model, material properties and numerical formulation were used for all three seasons so that differences were primarily due to seasonal boundary conditions.

Mesh Generation and Mesh Independence Study

A free tetrahedral mesh was generated in COMSOL Multiphysics 5.6 with local and boundary layer refinement, producing 486,000 elements and 108,000 degrees of freedom with element qualities of 0.18, 0.68 and 1.00 (minimum, average and maximum). Mesh independence for the dry, harmattan and rainy seasons used coarse **(**198,000**)**, intermediate (486,000) and fine **(**812,000 elements) meshes over 35 min (2100 s). For the dry season, maximum outlet velocities were 27.1, 27.7, and 27.9 m/s and maximum temperatures were 412.9, 415.8 and 416.7 K**,** with intermediate to fine changes of 0.72% and 0.22%**,** calculated using Relative change (%) = |(X_fine − X_coarse)/X_fine| × 100. Since both changes were below the 1% criterion, the 486,000-element mesh was selected for the final dry, harmattan and rainy season simulations in Kano, Northwestern Nigeria**.**

Table 2: Mesh Independence Study for the Representative Dry Season Simulation

Mesh level	Number of elements	Minimum mesh quality	Average mesh quality	Maximum Outlet Velocity (m/s)	Maximum Temperature (K)	Relative Change
Coarse	198,000	0.15	0.64	27.1	412.9	—
Intermediate	486,000	0.18	0.68	27.7	415.8	2.17% velocity; 0.69% temperature
Fine	812,000	0.20	0.71	27.9	416.7	0.72% velocity; 0.22% temperature

Based on the mesh-independence analysis, the intermediate mesh was adopted for all subsequent dry, harmattan, and rainy-season simulations. Using the same mesh ensured consistency in the numerical comparison of the seasonal airflow and temperature distributions.

Theoretical Framework

The theoretical framework of this analysis is based on Navier Stokes equations which govern the conservation of momentum in fluid motion. The airflow behavior and the time dependent temperature distribution within the flow domain were modeled and simulated using the fundamental equations of conservatives, momentum and energy (Patterson, 2018; Adair & Jaeger, 2019). For the symmetric three dimensional flow domain, the resulting transient equations governing fluid flow and heat transfer were formulated in an inertial frame of reference (Patterson, 2018; Adair & Jaeger, 2019; Agyeman *et al.,* 2023; Rahmat *et al.,* 2025; Kidane *et al.,* 2025). These equations are:

Heat Transfer in Solid

This equation represents heat conduction in a solid material. It states that the rate of change of thermal energy stored in the solid with time plus the divergence of the heat conducted through the solid is equal to the internal heat generation within the solid plus any external heat source applied (Patterson, 2018; Adair & Jaeger, 2019; Agyeman *et al.,* 2023; Rahmat *et al.,* 2025; Kidane *et al.,* 2025).

$$d_z \rho \mathrm{Cp} \frac{\partial \mathrm{T}}{\partial \mathrm{t}} + \nabla \cdot (-\mathrm{k}\nabla \mathrm{T}) = d_z \mathrm{Q} + q_0 \qquad (1)$$

Heat Transfer in Fluid

It accounts for the time rate of change of thermal energy in the fluid, the convective transport of heat due to fluid motion and heat conduction within the fluid. These effects are balanced by internal heat generation, external heat sources and additional heat produced due to viscous dissipation (Patterson, 2018; Adair & Jaeger, 2019; Agyeman *et al.,* 2023; Rahmat *et al.,* 2025; Kidane *et al.,* 2025).

$$d_z \rho \mathrm{Cp} \frac{\partial \mathrm{T}}{\partial \mathrm{t}} + \rho \mathrm{Cp} \cup \cdot \nabla \mathrm{T} + \nabla \cdot (-\mathrm{k}\nabla \mathrm{T}) = \mathrm{Q} + q_0 + d_z \mathrm{Qvd} \qquad (2)$$

Heat Flux (Inward)

The inward heat flux is represented by a general heat source term which accounts for heat supplied to the domain from an external source such as solar radiation (Patterson, 2018; Adair & Jaeger, 2019; Agyeman *et al.,* 2023; Rahmat *et al.,* 2025; Kidane *et al.,* 2025).

$$Q_0 = Q \qquad (3)$$

Heat Transfer in Porous Media

It states that the sum of internal heat generation, external heat sources, and viscous dissipation is equal to the rate of change of effective thermal energy stored in the porous medium plus the divergence of heat conducted through the porous structure using an effective thermal conductivity (Patterson, 2018; Adair & Jaeger, 2019; Agyeman *et al.,* 2023; Rahmat *et al.,* 2025; Kidane *et al.,* 2025).

$$d_z (\rho CP)_{eff} \frac{\partial \mathrm{T2}}{\partial \mathrm{t}} + \nabla \cdot (-d_z K_{eff} \nabla \mathrm{T2}) = d_z \mathrm{Q} + q_0 + d_z \mathrm{Qvd} \qquad (4)$$

Velocity Boundary Condition

The velocity vector is prescribed as a uniform inlet velocity acting normal to the boundary surface with magnitude equal to the specified inlet velocity (Patterson, 2018; Adair & Jaeger, 2019; Agyeman *et al.,* 2023; Rahmat *et al.,* 2025; Kidane *et al.,* 2025).

$$U = -U_0 \cap \quad (5)$$

RESULTS AND DISCUSSION

This section analyzes how seasonal variations affects wind velocity outlet and temperature distribution and what those changes means for performance of the solar dryer.

Results

The wind velocity outlet and temperature distribution seasonal performance of the system was evaluated during the dry season, harmattan season and rainy season to assess the dryer efficiency under different environmental conditions. These seasons present good weather patterns ranging from high solar intensity and lower humidity in the dry season to dust, higher humidity with reduced solar radiation in the rainy season and cooler condition during harmattan season. These results presented provide a comparative analysis of dryer's behavior across all the three seasons highlighting the impact of seasonal changes on drying efficiency and overall system performance.

Dry Season

In figures (1a) at 35 minutes, with the average wind speed of 7.86 m/s of the season used to predict the airflow velocity, it is noticed that the air flow in the dryer has become completely developed. The velocity profile matches perfectly with the profile at that time showing uniform flow from the inlet vain into the drying chamber. Even then, the highest speed (yellow red region, 27.9 m/s) still lies in the upper part of the outlets along with lower speeds in other portions because of resistance. However, the mean target of air flow manifests the steady state process achieved in the system which offers constant convective air flow appropriate for drying. At 35 minutes (2100 s) as shown in figure (1b), the average temperature of 36 ^{o}C of the season was used which shows that the temperature contours remain very high with peak temperatures of 416.71 K showing a strong changes in contour shape and high temperature distribution. This indicates that the system has reached a uniform steady thermal state where heat transfer patterns are established and further time has little effect on the overall temperature field.

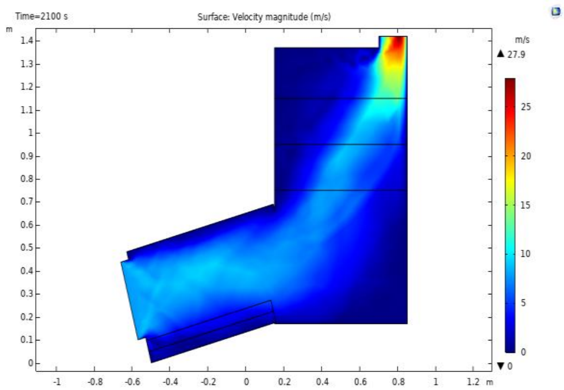

Figure (1a): Velocity Magnitude

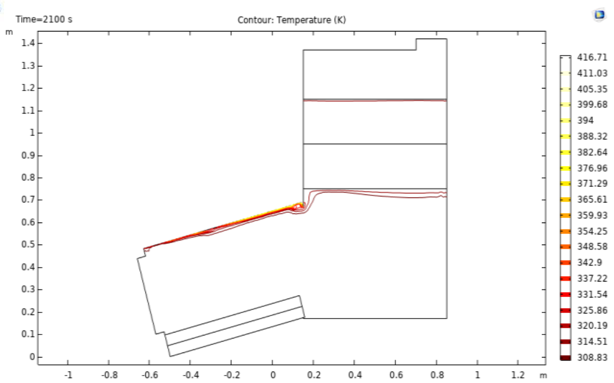

Figure (1b): Contour Temperature

Harmattan Season

At time 35 minutes as shown in (figure 2a), with the average wind speed of 6.56 m/s of the season used to predict the airflow velocity, the results show that the velocity distribution is uniformed showing peak velocities of around 23.5 m/s near the outlet and lower velocities throughout the rest of the channel. By 35 minutes as shown in figure (2b), the average temperature of 31.75 oC of the season was used to predict the temperature distribution. The results show that the contour pattern have slightly changed indicating that the thermal field has reached a steady state distribution of heat. The temperature distribution of 399.19 K was found reflecting stabilized heat transfer and sustained thermal equilibrium within the system.

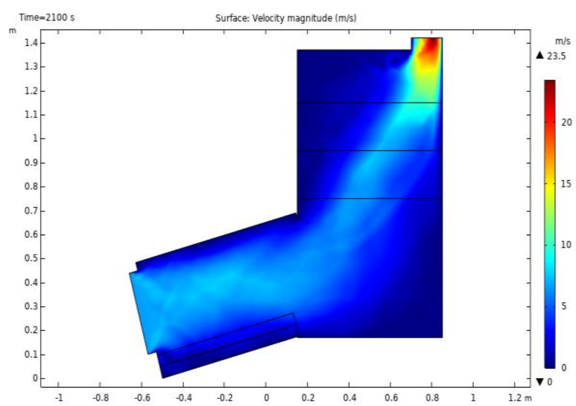

Figure (2a): Velocity Magnitude

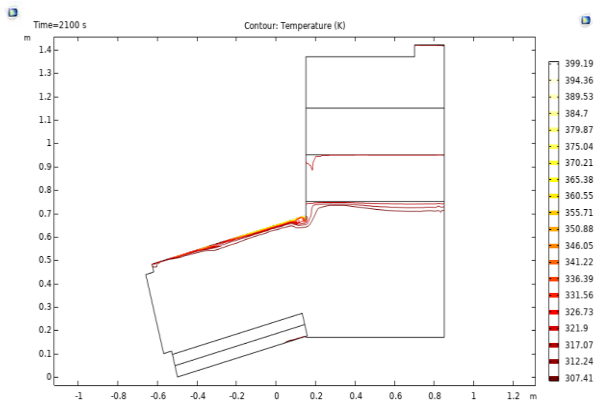

Figure (2b): Contour Temperature

Rainy Season

The velocity magnitude at 35 minutes as shown in figure (3a), with the average wind speed of 6.4 m/s of the season used to predict the airflow velocity, the results show its velocity distribution and velocities range from near 0 m/s in stagnant zones up to 22.8 m/s at the outlet along the duct showing that the flow has developed and spread through the system. In figure (3b) 35 minutes, the average temperature of 32 oC of the season was used to predict the temperature distribution. The contours show that the temperature distribution of 388.15 K was recorded showing the heat spreading in the system.

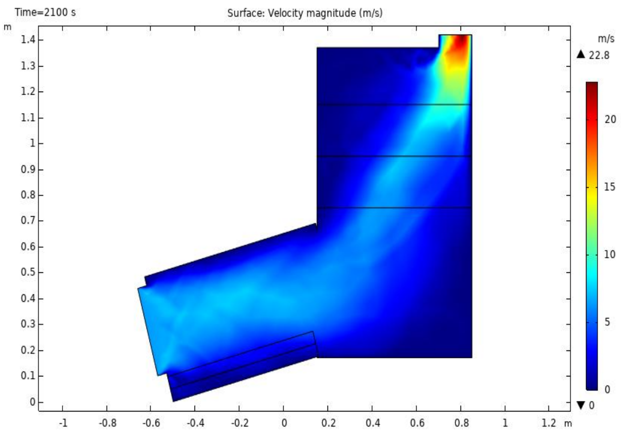

Figure (3a): Velocity Magnitude

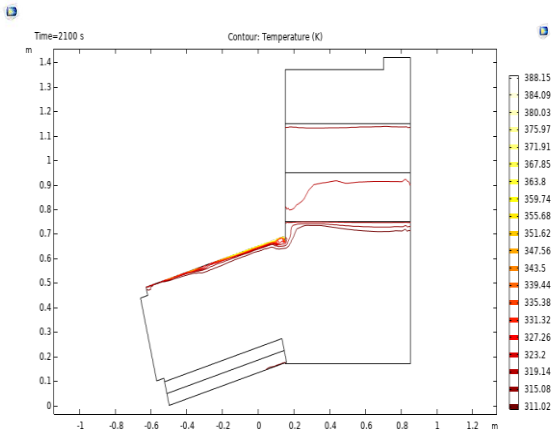

Figure (3b): Contour Temperature

Discussion

The numerical results show a clear seasonal pattern in the predicted airflow and thermal fields. At 35 min, the maximum outlet velocity was highest during the dry season (27.9 m/s) followed by the harmattan season (23.5 m/s) and the rainy season (22.8 m/s). Relative to the dry season, the predicted maximum outlet velocity decreased by 15.8% during harmattan and by 18.3% during the rainy season. The corresponding maximum predicted temperatures were 416.71 K (143.56 °C), 399.19 K (126.04 °C) and 388.15 K (115.00 °C) respectively. Thus, the dry season peak temperature was 17.52 K higher than the harmattan value and 28.56 K higher than the rainy season value. This consistent reduction indicates that the seasonal boundary conditions imposed in the model substantially affected both airflow intensity and the predicted thermal field.

The observed airflow and temperature patterns are qualitatively consistent with previous CFD studies of solar dryers which similarly reported that airflow distribution and thermal conditions within the drying chamber are strongly dependent on the dryer configuration and operating conditions. Demissie *et al.* (2019) reported mean airflow velocities of approximately 0.14 m/s on the lowest rack shelf and 0.12 m/s on the other shelves together with a steady chamber temperature of about 315 K after approximately 35 min. In the this study, the peak dry season temperature of 416.71 K was 101.71 K higher than the 315 K chamber operating temperature reported by Demissie *et al.* (2019). However, this difference should not be interpreted as a direct performance advantage because the two studies used different dryer geometries, boundary conditions, airflow definitions and temperature metrics. The comparison nevertheless provides a direct numerical benchmark showing that this CFD model predicts the same general transient evolution toward an established thermal field while operating at a substantially different temperature level.

Similarly, Aukah *et al.* (2020) reported spatially homogeneous airflow and temperature distributions in a CFD analysis of a hybrid solar-biomass dryer and experimental validation showed a small temperature variation of about 0.7 °C between simulated and measured results. Beyene (2017) also demonstrated using CFD that dryer performance is governed by the interaction between airflow and thermal conditions and reported average thermal efficiencies of 50.6% under clear sky conditions and 36.8% under partially overcast conditions. These findings support the comparative pattern observed in this research more favorable thermal and airflow conditions produced higher predicted performance indicators whereas less favourable seasonal conditions produced lower values. Nevertheless, because this study did not calculate thermal efficiency and did not include experimental measurements, its results should be compared primarily in terms of airflow and temperature distributions rather than efficiency or validation accuracy.

Generally, the dry season produced the highest predicted outlet velocity and peak temperature distribution followed by the harmattan and rainy seasons. Despite seasonal variations, the indirect solar dryer demonstrated acceptable performance throughout the year confirming its potential for continuous agricultural drying.

CONCLUSION

In this study, the seasonal performance of an indirect solar dryer was numerically investigated using CFD. At 35 min, the predicted maximum outlet velocities were 27.9 m/s, 23.5 m/s and 22.8 m/s for the dry, harmattan and rainy seasons respectively while the corresponding maximum predicted temperatures were 416.71 K, 399.19 K and 388.15 K. The dry season therefore produced the highest predicted airflow velocity and temperature distribution followed by the harmattan and rainy seasons. These findings indicate that seasonal environmental conditions influence the airflow and thermal behaviour of the dryer. Further work should include experimental validation and investigation of design modifications that can improve dryer performance during periods of reduced solar availability.

CONTRIBUTION TO KNOWLEDGE

i. The study provides seasonal performance data for indirect solar dryers improving efficiency of agricultural drying throughout the year.
ii. It shows the relationship between airflow, temperature and drying efficiency supporting better dryer design and performance.
iii. It validates CFD based simulation as an economical solution for predicting and enhancing solar dryer performance before construction.

ACKNOWLEDGEMENT

The authors like to acknowledge the department of Physics, Bayero University, Kano for supporting this research through the project entitled: CFD Modeling, Validation Design,

Construction and Performance Evaluation of an Indirect Solar Dryer with Thermal Storage for Drying Agricultural Products.

REFERENCES

Agyeman, Emmanuel Kwadwo Kale; Duret, Steven; Flick, Denis; Laguerre, Onrawee; Moureh, Jean. (2023). Computational Modelling of Airflow and Heat Transfer during Cooling of Stacked Tomatoes: *Optimal Crate Design. Energies, 16, 2048.* https://doi.org/10.3390/en16042048.

Alvarado-Rodríguez, Carlos Eduardo; Díaz-Damacillo, Lamberto; Plaza, Eric; & Di G. Sigalotti, Leonardo. (2023). Smoothed particle hydrodynamics simulations of porous medium flow using Ergun's fixed-bed equation. *Water, 15(13), 2358.* https://doi.org/10.3390/w15132358.

Aukah, J., Muvengei, M., Ndiritu, H., & Onyango, C. (2020). Prediction of airflow and temperature distribution in hybrid solar-biomass dryer using computational fluid dynamics. *Journal of Sustainable Research in Engineering*, 4(3), 76–89.

Beyene, T. (2017). Design and Simulation of Forced Solar Coffee Dryer Using Computational Fluid Dynamics (CFD). *Journal of Science, Technology and Arts Research*, 6(3), 1–17. https://doi.org/10.20372/star.v6i3.406

Demissie, P., Mesele, H., Amanuel, K., Hailesilassie, A., Gebrehiwot, M., & Vanierschot, M. (2019). Design, development and CFD modeling of indirect solar food dryer. *Energy Procedia*, 158, 1128–1134. https://doi.org/10.1016/j.egypro.2019.01.278.

Desmond Adair and Martin Jaeger (2019) An Efficient Strategy to Deliver Understanding of Both Numerical and Practical Aspects When Using Navier-Stokes Equations to Solve Fluid Mechanics Problems. *Fluids, 4(4), 178.* DOI: DOI: https://doi.org/10.3390/fluids4040178

Halefom Kidane, Istvan Farkas, Janos Buzás (2025) Modeling airflow dynamics in solar drying chambers: a comprehensive review of CFD applications. *Discover Applied Sciences*, DOI: https://doi.org/10.1007/s42452-025-06894-6.

Li, Xin; Zhong, Wei; Liao, Yuxuan; Xu, Ke; Tao, Guoliang; & Kagawa, Toshiharu. (2016). Determination of pressure drop for air flow through sintered metal porous media using a modified Ergun equation. *Advanced Powder Technology, 27(4)*, 1134–1140. https://doi.org/10.1016/j.apt.2016.03.024.

Marcato, A., Boccardo, G., & Marchisio, D. (2022). From computational fluid dynamics to structure interpretation via neural networks: An application to flow and transport in porous media. *Industrial & Engineering Chemistry Research, 61(24*), 8530–8541. https://doi.org/10.1021/acs.iecr.1c04760.

Muhammad Aqil Afham Rahmat, Adnan Ibrahim, Muhammad Amir Aziat Ishak, Ubaidah Syafiq, Khaled M. Al-Aribe (2025). Numerical investigation of thermal and airflow profiles in diverse solar dryer chamber configurations. *Case Studies in Thermal Engineering, 73, 106612.* https://doi.org/10.1016/j.csite.2025.106612.

Müller, L. C. (2024). Enhancing post-harvest preservation through improved and even solar drying: A case study in Bhutan. *Department of Energy Sciences, Lund University.* https://doi.org/10.1093/fqsafe/fyy010.

Olabode, O.H., Musa, J.G., Musa, H., & Samuel, A.A. (2023) Assessing the Influence of Agro-climatic Factors on Solar Dryer Performance: Review Study of Zaria Kaduna State, Nigeria. *International Journal of Academic Multidisciplinary Research*, 7(11), 109–125.

Patterson, J. (2018). Effect of drying technologies on the biochemical properties of Stolephorus commersonnii. *Food Quality and Safety*, 2(3), 153–158.

Zhong, Wei; Li, Xin; Tao, Guoliang; & Kagawa, Toshiharu. (2015). Measurement and determination of friction characteristic of air flow through porous media. *Metals, 5(1)*, 336–349. https://doi.org/10.3390/met5010336.